Morphometric analysis of small-scale lobate scarps on the Moon using data from the Lunar Reconnaissance Orbiter

M. E. Banks,[1] T. R. Watters,[1] M. S. Robinson,[2] L. L. Tornabene,[1] T. Tran,[2] L. Ojha,[3] and N. R. Williams[2]

Received 17 August 2011; revised 6 December 2011; accepted 11 December 2011; published 7 March 2012.

[1] Prior to Lunar Reconnaissance Orbiter (LRO), the morphology and dimensions of only a limited number of lobate scarps, all located near the equator (within 21°), had been characterized. Topography derived from LRO Camera stereo images and Lunar Orbiter Laser Altimeter (LOLA) ranging is used to measure the relief and analyze the morphology of previously known and newly detected low and high latitude lobate scarps. The asymmetric profiles and maximum slopes on scarp faces (~5° to 29°) of lunar lobate scarps are similar to those of lobate scarps observed on Mars and Mercury. Scarp lengths range from ~0.6 to 21.6 km (mean = ~6.0 km, median = ~4.4 km, n = 79), and measured relief ranges from ~5 to 150 m (mean = ~35 m, median = ~20 m, n = 26). Assuming a range of 20° to 40° for the fault plane dip, estimated lower limits for the horizontal shortening (S) expressed by the lobate scarp thrust faults range from ~10 to 410 m. The range in S estimated for the lunar scarps is roughly an order of magnitude lower than estimates of S for lobate scarp thrust faults on Mars and Mercury. The relatively small range of S estimated for the growing number of well-characterized lunar scarps is consistent with a small amount of global contraction.

Citation: Banks, M. E., T. R. Watters, M. S. Robinson, L. L. Tornabene, T. Tran, L. Ojha, and N. R. Williams (2012), Morphometric analysis of small-scale lobate scarps on the Moon using data from the Lunar Reconnaissance Orbiter, *J. Geophys. Res.*, *117*, E00H11, doi:10.1029/2011JE003907.

1. Introduction

[2] Contractional tectonic landforms found on the Moon include wrinkle ridges and lobate scarps. Wrinkle ridges are complex landforms that only occur in mare basalts. They commonly consist of a broad arch with superposed narrow asymmetric ridges, and their origin is attributed to basin-localized compressional stresses that induce folding and/or thrust faulting [i.e., *Strom*, 1972; *Howard and Muehlberger*, 1973; *Lucchitta*, 1976, 1977; *Wilhelms*, 1987; *Plescia and Golombek*, 1986; *Watters*, 1988; *Golombek et al.*, 1991, 2001; *Schultz*, 2000; *Watters*, 2004]. This study focuses on lobate scarps which are morphologically simple, small-scale landforms with relatively steeply sloping scarp faces and more gently sloping back limbs [i.e., *Strom et al.*, 1975; *Watters*, 1993; *Watters and Robinson*, 1999; *Watters et al.*, 2000, 2009; *Watters and Johnson*, 2010; *Watters et al.*, 2011]. On the Moon, lobate scarps are observed both in the mare and, more commonly, in the highlands [*Schultz*, 1976; *Binder*, 1982; *Binder and Gunga*, 1985; *Watters and Johnson*, 2010]. They are the most common tectonic feature on the farside [*Watters and Johnson*, 2010] and are believed to be among the youngest lunar landforms [*Binder*, 1982; *Binder and Gunga*, 1985; *Watters et al.*, 2010; *Watters and Johnson*, 2010]. Lobate scarps are the result of low-angle thrust faults [*Howard and Muehlberger*, 1973; *Lucchitta*, 1976; *Binder*, 1982; *Binder and Gunga*, 1985]. They are observed to crosscut impact craters and the vergence direction is frequently oriented upslope (Figure 1) [*Mattingly et al.*, 1972; *Schultz*, 1976; *Masursky et al.*, 1978]. In plan view they are often lobate, form linear or arcuate and commonly en echelon stepping scarp segments, and may be associated with scarp complexes or clusters consisting of a number of individual scarps. The vergence of scarps sometimes changes along strike indicating reversals in the dip direction of the underlying faults of individual segments. Results from elastic dislocation modeling constrained by topography of lobate scarp faults on Mars and Mercury, and a lobate scarp on asteroid 433 Eros named Hinks Dorsum, indicate that underlying thrust faults have planar geometries [*Schultz and Watters*, 2001; *Watters and Schultz*, 2002; *Watters et al.*, 2002, 2011].

[3] Prior to Lunar Reconnaissance Orbiter (LRO) observations, lobate scarps were largely detected only in equatorial regions because of limited Apollo Panoramic Camera and high resolution Lunar Orbiter coverage with optimum lighting geometry (less than 10% of the lunar surface) [*Binder*, 1982; *Binder and Gunga*, 1985; *Watters and Johnson*,

[1]Center for Earth and Planetary Studies, National Air and Space Museum, Smithsonian Institution, Washington, D. C., USA.
[2]School of Earth and Space Exploration, Arizona State University, Tempe, Arizona, USA.
[3]Lunar and Planetary Laboratory, University of Arizona, Tucson, Arizona, USA.

0148-0227/12/2011JE003907

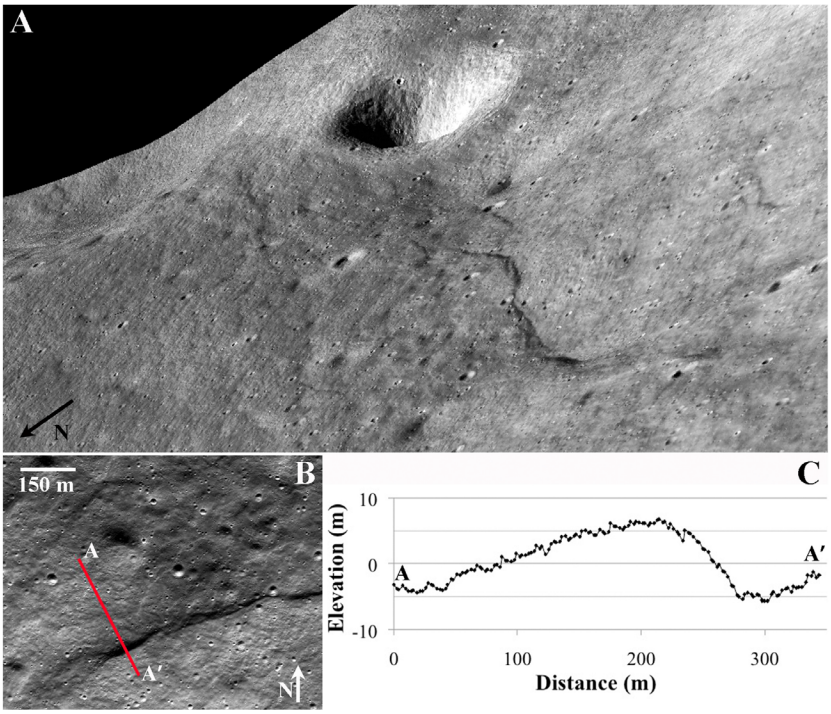

Figure 1. (a) Perspective view from a LROC NAC DTM (NAC images M139804021LE, M139804021RE, M139817589LE, and M139817589RE) of lobate scarp Simpelius-1 (∼73.56°S, 13.04°E) located on the wall of Simpelius crater (vertical exaggeration is 4:1). The vergent side of the scarp is oriented upslope. The DTM has a horizontal spatial scale of 2 m/post and elevations are referenced to a sphere of 1,737,400 m. The vertical precision error is expected to be ∼5 m. The length of the scarp in this image is ∼1 km. (b) Nadir view of Simpelius-1. The red line marks the location of the profile in C (NAC image M139804021LE). (c) Detrended profile derived from the DTM in Figure 1a. The maximum relief of this scarp is 13 ± 5 m.

2010]. Thus, our previous understanding of lobate scarp morphology and scale was based on measurements of a limited number of low-latitude scarps. Lengths of the scarps were measured on Apollo Panoramic Camera images and range from 0.7 to 22.3 km [*Binder and Gunga*, 1985; *Watters and Johnson*, 2010] with a mean length of ∼9 km (n = 67) [*Binder and Gunga*, 1985]. Previous measurements of lobate scarp relief were acquired for 9 low-latitude scarp segments (within 21° of the equator), and range from ∼6 to 80 m (mean maximum relief of ∼32 m) [*Watters and Johnson*, 2010]. However, the relief of these scarps was primarily determined from shadow measurements with limited accuracy acquired from Apollo-era photography.

[4] Lunar Reconnaissance Orbiter Camera (LROC) images and Lunar Orbiter Laser Altimeter (LOLA) ranging enable detection and detailed morphological analysis of lobate scarps at all latitudes. To date, previously undetected scarps have been identified in LROC images and mosaics in more than 75 different locations, more than 20 of which occur at latitudes greater than 60° [*Banks et al.*, 2011], and appear to be globally distributed [*Watters et al.*, 2010]. We present the results of a detailed characterization of the relief and morphology of a larger sampling of the population of lobate scarps. Outstanding questions include what is the range of maximum relief of the lobate scarps? Is their size and structural relief consistent with estimates of the global contractional strain? What is the range of horizontal shortening expressed by lunar scarps and how does this range compare with that found for planetary lobate scarps?

[5] LROC mosaics and stereo-derived digital terrain models (DTMs) and LOLA data are used to measure the relief and characterize the morphology of lobate scarps ranging in latitude from ∼86°S to 88°N and occurring on both the nearside and farside (Figure 2). Lunar examples are compared to lobate scarps on Mars, Mercury, and Eros.

2. Data and Methods

[6] LROC consists of a Wide-angle Camera (WAC) which provides global imaging at a scale of 100 m/pixel, and two Narrow Angle Cameras (NACs) which provide up to 0.5 m-scale panchromatic images over a combined 5-km swath [*Robinson et al.*, 2010]. Five DTMs derived from LROC NAC stereo pairs were analyzed to obtain measurements of maximum relief for 5 lobate scarps (Figures 1 and 3 and Table 1). The spatial resolution of the DTMs ranges from ∼2 to 4 m/post and the vertical precision error ranges from ∼2 to 5 m (see Table 1) [*Tran et al.*, 2010].

[7] The LOLA instrument transmits 5 beams, each illuminating a 5-m spot from a 50-km altitude orbit. Five parallel profiles, ∼12 m apart, are created with individual observations separated by ∼56 m along each profile [*Smith*

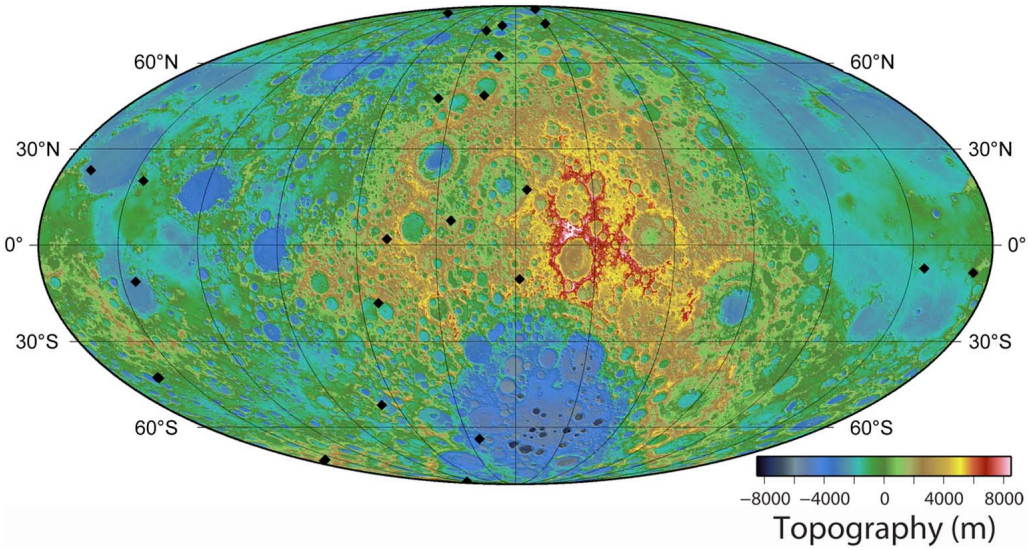

Figure 2. Locations of the 26 lobate scarps measured for their relief in this study (black diamonds, see Table 1) plotted on a Mollweide equal area projection of a shaded relief map merged with a global LROC WAC stereo derived DTM [*Scholten et al.*, 2012]. The projection is centered on the lunar farside at 180°E longitude. Lines of longitude are 30 degrees apart.

et al., 2010]. LOLA ranging has a vertical precision of up to ±0.1 m. Data points were acquired using the Lunar Orbital Data Explorer (http://ode.rsl.wustl.edu/).

[8] LOLA profiles were used to measure the relief of 21 scarp segments where the profiles traverse the scarps at orthogonal or near to orthogonal angles (Figures 4 and 5 and Table 1). Because of LRO's polar orbit, only principally E-W trending scarps with sufficient LOLA and NAC coverage were examined with LOLA topography. All available LOLA tracks along the length of each scarp were examined and the relief of the scarp was measured in each profile. We report only the greatest relief found for each scarp along its length. However, it should be noted that this is not necessarily the maximum relief as the LOLA tracks do not provide continuous coverage along the entire length of each scarp. When measuring relief using DTMs, profiles along the entire length of each scarp were obtained enabling determination of the maximum relief. Thus, the relief measured from LOLA topography and from DTMs is described as "greatest measured relief" and "maximum relief" respectively. For lobate scarps located on slopes, such as the slopes of crater walls, the relief was measured using detrended topographic profiles. This was accomplished by subtracting a least squares linear fit to the topographic data across the scarp face and back-scarp terrain.

[9] Lengths were measured for 79 scarp segments (Table 2). Where possible, scarp lengths were measured using NAC mosaics. In cases where the full extent of the scarp has not yet been covered by NAC imagery, a WAC 100 m global mosaic was used in combination with NAC imagery to estimate scarp lengths. Slopes were determined along the steepest section of the scarp face in profiles showing the greatest relief for each scarp. When necessary, the length of the run was adjusted by measuring the angle between the orientation of the profile and a line orthogonal to the scarp face, and used to compute a corrected slope.

[10] Because of the scale of the lobate scarps, they are often only detected and confirmed in high resolution LROC NAC images. As of the time of this writing, only about 35% of the surface of the Moon had been covered by NAC images. Although lobate scarps have now been identified in over 75 individual locations on the Moon, these scarps are likely only a sample of the total population. Of these scarps, only those with sufficient NAC coverage at the time of this study were measured.

3. Results

3.1. Scarp Morphology and Length

[11] The lunar lobate scarps typically exhibit asymmetric profiles with relatively steeply sloping scarp faces and more gently sloping back limbs (Figures 1, 3, 4, and 5). Thus they share similar basic morphological elements with lobate scarps on Mars, Mercury, and Eros [i.e., *Strom et al.*, 1975; *Watters*, 1993; *Watters and Robinson*, 1999; *Watters et al.*, 2000, 2009; *Watters and Johnson*, 2010; *Watters et al.*, 2011]. The maximum slope on the scarp faces (n = 26) ranges from ∼5° to 29° with a mean of ∼13°, and a median of ∼12° (Figure 6 and Table 1). This range of slopes, as well as the mean slope, is generally comparable to maximum slopes reported for lobate scarps on Mars and Mercury (up to 17°) [i.e., *Watters et al.*, 1998; *Watters and Robinson*, 1999] and Hinks Dorsum (∼20°) [*Watters et al.*, 2011].

[12] Lengths for 79 lobate scarp segments were measured in LROC mosaics. Results range from ∼0.6 to 21.6 km with an average length of ∼6.0 km (median = 4.4 km) (Table 2 and Figure 7). Of the scarp segments measured to date, the longest (>10 km, n = 11) all occur within 33 degrees of the equator with the exception of one scarp segment (Figure 7b). The significance of this observation is not yet clear. The range of lengths of the population of scarps measured here is consistent with the range reported in previous studies

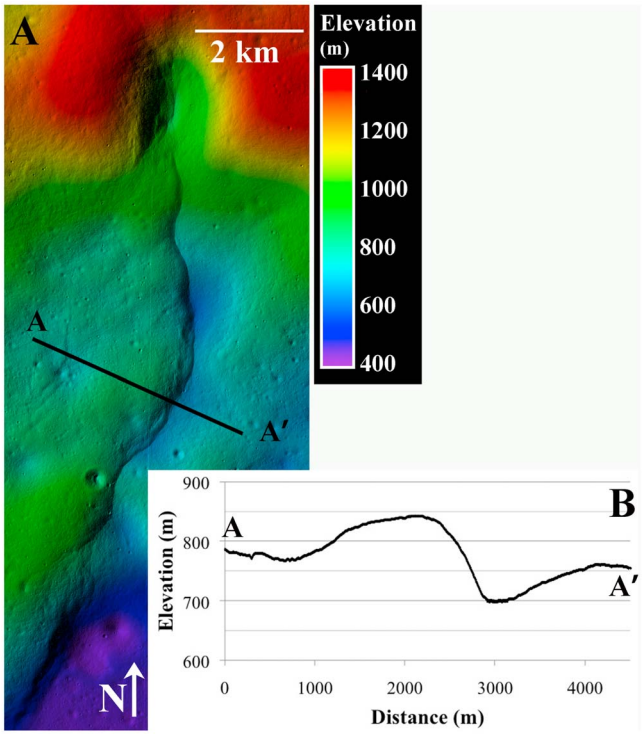

Figure 3. (a) DTM from NAC stereo images (M143459779LE, M143459779RE, M143452995RE, and M143452995LE) of lobate scarp Racah X-1 (10.06°S, 178.10°E). The black line marks the location of the profile in Figure 3b. The DTM has a horizontal spatial scale of 2 m/post and a vertical precision of ∼5 m. Elevations are referenced to a sphere of 1,737,400 m. (b) Profile across Racah X-1 derived from the DTM in Figure 3a. With a maximum relief of 150 ± 5 m, this newly identified lobate scarp is the largest measured to date.

[*Binder and Gunga*, 1985; *Watters and Johnson*, 2010]. Combining our measurements with those from *Binder and Gunga* [1985] and *Watters and Johnson* [2010], we find that the lobate scarps are typically tens of kilometers or less in length. They are shorter than lobate scarps on Mars and Mercury (typically up to hundreds of kilometers) [*Strom et al.*, 1975; *Watters*, 2003; *Solomon et al.*, 2008; *Watters et al.*, 2009; *Watters and Nimmo*, 2010] but comparable in length to Hinks Dorsum (∼18 km) [*Watters et al.*, 2011].

3.2. Scarp Relief

[13] Relief of the 26 lobate scarps analyzed with NAC DTMs and LOLA profiles ranges from ∼5 to 150 m with a mean relief of ∼35 m (median = ∼20 m) (Figure 8 and Table 1); the mean relief will likely increase as more NAC DTMs become available and the maximum relief, as opposed to the greatest measured relief, for each scarp can be determined (maximum relief currently reported for 5 scarps; see Table 1). All but five of the scarps measured so far have a relief of less than 41 m. While the scarps with the largest relief (≥64 m; n = 5) measured so far are located near the equator (within 20°) and at very high latitudes (polewards of 84°), scarps with a relief up to ∼20–30 m are observed at nearly all latitudes (Figure 8b). The range of relief reported here encompasses the range of relief previously reported for only nine low-latitude scarp segments [*Watters and Johnson*, 2010; *Watters et al.*, 2010]. The current data, as well as the previously reported data, collectively indicate that lunar lobate scarps, as a whole, typically exhibit tens of meters of relief. Lunar lobate scarps are typically smaller than those observed on Mercury [*Strom et al.*, 1975; *Solomon et al.*, 2008; *Watters et al.*, 2009; *Watters and Nimmo*, 2010] and Mars [*Watters*, 2003], some of which have maximum reliefs of over 1 km, but are comparable to Hinks Dorsum and two smaller subsidiary scarps on Eros which range in maximum relief from ∼25 to 60 m [*Watters et al.*, 2011].

[14] Racah X-1 is a newly identified scarp located at 10.06°S, 178.10°E (Figure 3), just west of the impact crater Racah X. This is the largest lunar lobate scarp measured to date with a relief of ∼150 ± 5 m (Table 1). Racah X-1 is located in a heavily cratered area of the farside highlands and crosscuts multiple heavily degraded craters. Because of the undulating topography, measurements were constrained to locations where the relief could most likely be attributed to structural relief rather than the influence of pre-existing topography. This scarp appears to be part of a complex of scarps that extends for tens of kilometers with several additional segments located to the north (see Table 2). Due to the primarily N-S orientation, the relief of other scarp segments could not be measured accurately with LOLA profiles. Racah X-1 has a steeply sloping scarp face with a maximum measured slope of 29°. This is only slightly higher than the maximum scarp-face slope measured for Lee-Lincoln, the second largest scarp measured to date with a relief of ∼130 m (Table 1). Several linear landforms oriented parallel to the trend of the scarp, some of which appear to be flat-floored troughs bounded by inward facing slopes, may be graben or evidence of extension associated with Racah X-1. Profiles acquired from a NAC DTM (Figure 3) indicate that the linear landforms are located in the elevated back-scarp terrain, some clustered near the crest of the lobate scarp. Extensional structures associated with lobate scarps, often occurring in the back-scarp terrain (i.e., Lee-Lincoln scarp), have been observed in additional LROC NAC images [*Watters et al.*, 2010, 2012]. Extensional stresses are thought to result from uplift and flexural bending caused by slip on the underlying thrust fault related to the lobate scarp [*Wolfe et al.*, 1981; *Watters et al.*, 2010, 2012].

[15] The high latitude scarp with the greatest relief measured so far is Shoemaker (86.24°S, 54.29°E) (Figure 4). This scarp is located within a degraded crater near the ∼48-km-diameter impact crater Shoemaker. Like several other newly identified lobate scarps, the entire length of Shoemaker is located on the crater wall. The length of the scarp is just over 3 km and its vergent side is oriented upslope. The relief is greater in the northern half of the scarp with a greatest measured relief of just over 80 m and a maximum slope on the scarp face of ∼17° (Table 1).

[16] Four high-latitude (polewards of 63°) primarily east-west-trending lobate scarps, in the low to moderate range of relief, are shown in Figures 1 and 5. Lyman V (63.46°S, 151.44°E) is found in intercrater plains near the edge of the South Pole Aitken Basin (Figure 5). It is named after the nearby ∼37-km-diameter impact crater Lyman V and spans

Table 1. Lobate Scarp Relief and Estimates of Shortening

Scarp Name (Informal)[a]	Latitude (°N)	Longitude (°E)	Relief (m)	Slope (degrees)	*S* Range (m) (θ = 20°–40°)
Lobate Scarps Analyzed Using LOLA (Greatest Measured Relief)[b]					
Avogadro-1	64.12	164.15	8	6	10–20
Bridgman C	47.28	138.78	9	8	10–30
Gregory	2.06	128.15	17	12	20–50
Henderson	7.77	152.07	14	12	20–40
Kugler	–51.34	108.02	11	6	10–30
Lalande A	−8.25	350.34	40	14	50–110
Litke (Lütke)	−17.91	123.30	5	6	~10
Lyman V	−63.46	151.44	17	9	20–50
Mädler	−10.90	31.80	36	18	40–100
Maurolycus-1	−41.79	14.84	24	8	30–70
Maurolycus-2	−41.58	14.40	40	19	50–110
Milankovič-1 (S1)	77.06	158.26	9	6	10–30
Nansen F	84.35	51.55	64	13	80–180
Poinsot	78.04	201.45	13	12	20–40
Riphaeus	−6.86	331.49	87	8	100–240
Rozhdestvenskiy-1	87.50	211.60	23	12	30–60
Shoemaker	−86.24	54.29	81	17	100–220
Simpelius-2	−74.03	8.83	6	5	10–20
Simpelius-3	−73.92	9.90	14	7	20–40
Virtanen	17.37	181.06	27	14	30–70
West-Serenitatis	23.50	7.52	38	10	50–100
Lobate Scarps Analyzed With LROC NAC DTMs (Maximum Relief)[c]					
Lee-Lincoln	20.27	30.56	130 ± 5	27	160–360
Racah X-1	−10.06	178.10	150 ± 5	29	180–410
Seares	74.51	147.11	16 ± 3	14	20–40
Simpelius-1	−73.56	13.04	13 ± 5	26	20–40
Slipher	48.22	160.56	21 ± 2	22	30–60

[a]Scarps are unofficially named after a large nearby crater or the crater within which they are located. The name is sometimes followed by a "−1," "−2," etc. to specify individual scarps within a cluster or complex of multiple individual scarps. "(S1)," "(S2)," etc. refers to separate segments of one individual scarp.

[b]LOLA ranging has a vertical precision of up to ±0.1 m.

[c]The spatial resolution of the DTM covering Seares scarp is 4 m/post. All other DTMs have a spatial resolution of 2 m/post. The vertical precision error for the DTMs covering the Lee-Lincoln, Simpelius-1, and Racah X-1 scarps is expected to be ~5 m. The vertical precision error for the DTMs covering Seares and Slipher scarps is ~3 m and ~2 m respectively [*Tran et al.*, 2010].

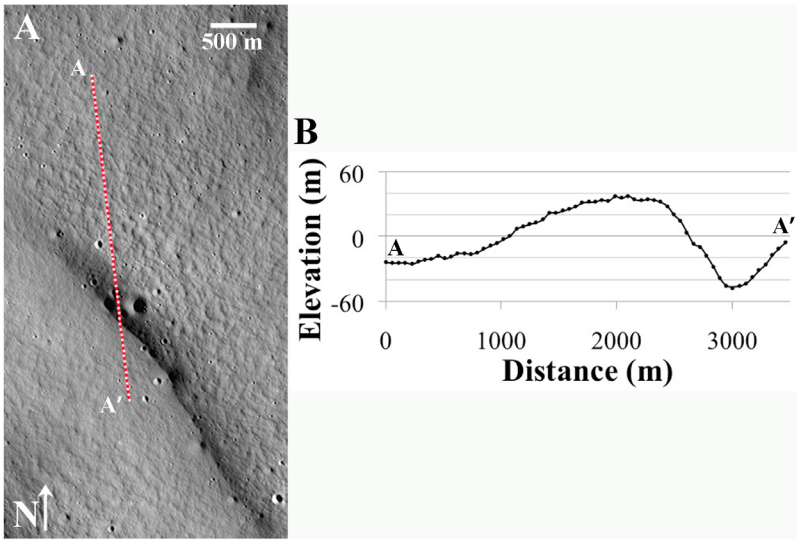

Figure 4. (a) High latitude lobate scarp Shoemaker (86.24°S, 54.29°E; NAC images M115979457RE and M115979457LE). The location of the LOLA track is indicated by a red line where it traverses the scarp. (b) Detrended LOLA profile (data from sensor 3) of Shoemaker scarp. This scarp has a greatest measured relief of 81 m. Elevations are referenced to a sphere of 1,737,400 m.

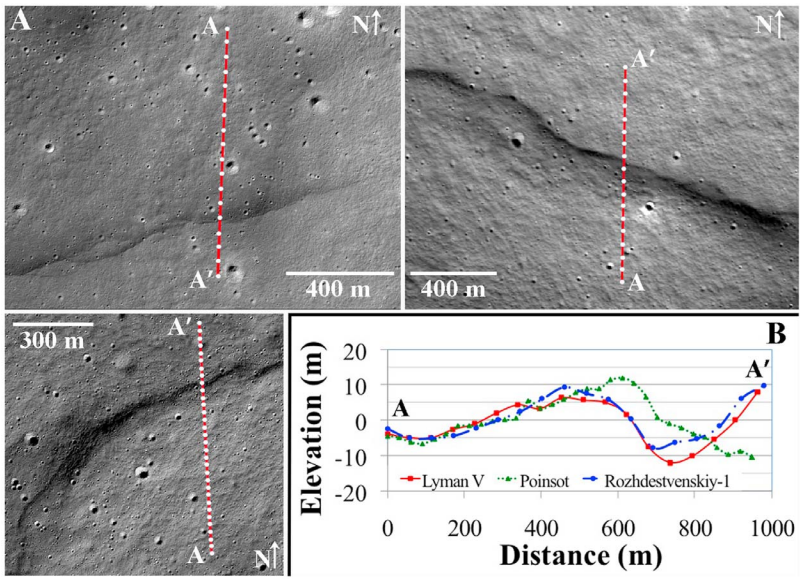

Figure 5. LOLA profiles of three high latitude lobate scarps newly identified in LROC imagery. (a) (top left) Lyman V (63.46°S, 151.44°E; NAC image M121225544RE). (top right) Rozhdestvenskiy-1 (~87.50°N, 211.60°E; NAC image M107957296RE). (bottom left) Poinsot (78.04°N, 201.45°E; NAC image M127960702RE). The location of the LOLA track is indicated by a red line where it traverses each lobate scarp. (b) Detrended LOLA profiles of the scarps shown in Figure 5a. Data from sensor 3 is shown for Lyman V and Rozhdestvenskiy-1 and data from sensors 3 and 4 is shown for Poinsot. Elevations are referenced to a sphere of 1,737,400 m.

2.46 km in length. Lyman V consists of one main scarp segment spanning 2.5 km in length. Simpelius-1 (~73.56°S, 13.04°E) is a cluster of small scarps, some forming en echelon stepping segments, located on the sloping wall of the ~70-km-diameter crater Simpelius (Figure 1). The scarps in this cluster are relatively small, typically less than ~1 km in length. In most cases the vergent side of the scarp segments is oriented upslope. The northernmost scarp is Rozhdestvenskiy-1 (~87.50°N, 211.60°E; Figure 5). This scarp is located on rim material along the wall of an impact crater named Rozhdestvenskiy (~180 km in diameter). Rozhdestvenskiy-1 appears to consist of at least two en echelon scarp segments, the longer of which has a length of ~3.40 km. Poinsot (78.04°N, 201.45°) is located in highlands material on the nearside just southeast of the ~65-km-diameter impact crater Poinsot (Figure 5). In plan view, it forms a broad arc curving slightly to the north-northwest with a length of 1.49 km. It consists of one scarp segment with a total length of 1.8 km. Despite variations in their characteristics and local geologic and topographic settings, all four of these scarps exhibit very similar asymmetric profiles (Figures 1 and 5). The greatest measured relief for all four scarps ranges from only ~13 to 23 m and the maximum slope on the scarp faces varies by only a few degrees (from 9 to 12°) with the exception of Simpelius-1 which has a maximum slope of 26° (Table 1).

3.3. Estimated Horizontal Shortening and Stress

[17] The horizontal shortening associated with lobate scarps can be estimated with a kinematic model of a thrust fault that propagates upward and breaks the surface. Using the measured relief (h) and a range of values for the fault plane dip (θ), we can estimate a range for the lower limit of horizontal shortening (S) by assuming it is a function of the relief of the scarp and the dip of the surface-breaking fault plane such that $S = h/\tan\theta$ [*Wojtal*, 1996; *Watters and Robinson*, 1999; *Watters et al.*, 2000]. From experimental results [*Byerlee*, 1978], terrestrial field measurements [i.e., *Jaeger and Cook*, 1979, *Brewer et al.*, 1980; *Gries*, 1983; *Stone*, 1985], and elastic dislocation modeling of thrust faults on Mars, Mercury, and Eros [i.e., *Schultz and Watters*, 2001; *Watters et al.*, 2002, 2011; *Grott et al.*, 2007], we conservatively assume a range in θ of 20° to 40° for the thrust faults associated with lunar scarps. It is also assumed that fault dips are generally uniform and fault geometries are planar based on terrestrial analogs [*Brewer et al.*, 1980; *Gries*, 1983; *Stone*, 1985], and that overthrusting is not significant; although if overthrusting is significant, the estimates reported here would still remain lower limits. Estimated lower limits for the horizontal shortening across the lunar scarp thrust faults range from ~10 to 410 m (Table 1). The range of horizontal shortening estimated for the growing number of well-characterized lunar examples is consistent with a small amount of contractional strain and a low amount of global radial contraction [*Watters et al.*, 2010]. Due to the lack of sufficient topographic data, the horizontal shortening of lunar lobate scarps has not been estimated previously. However, these results are consistent with the small amount of contractional strain and radial contraction estimated using the displacement-length (D-L) scaling relation of previously known lobate scarps reported by *Watters and Johnson* [2010] and updated in *Watters et al.* [2010]. For the same range in θ, these results are roughly an order of magnitude lower than the S estimated for lobate scarp thrust faults on both Mars and Mercury, which range from a few hundred meters to several kilometers (up to ~3–

Table 2. Lengths of Lobate Scarps[a]

Scarp Name (Informal)[b]	Latitude (°N)	Longitude (°E)	Length (km)
Avogadro-1	64.12	164.15	1.13
Avogadro-2	64.05	164.47	3.13
Bridgman C	47.28	138.78	2.32
Chappell-1 (S1)	56.56	181.06	5.25
Chappell-1 (S2)	56.68	181.19	3.59
Chappell-2 (S1)	58.21	181.97	6.03
Chappell-2 (S2)	58.61	182.14	4.27
De Vries-1 (S1)	−18.34	181.38	3.81
De Vries-1 (S2)	−18.43	181.48	2.13
Evdokimov N	32.36	207.44	4.24
Evershed S-1	33.00	197.10	19.61[c]
Evershed S-2	33.83	197.41	9.79[c]
Feokistov	32.02	140.49	4.08
Fowler	43.28	212.94	9.36
Gregory	2.06	128.15	11.33[c]
Henderson	7.77	152.07	4.87
Kondratyuk	−15.27	116.77	21.60
Korolev-1	2.95	195.36	18.75
Korolev-2	1.65	195.62	12.35
Kugler	−51.34	108.02	14.70[c]
Lalande A	−8.25	350.34	14.00[c,d]
Lebedev F	−45.14	115.42	9.58
Lee-Lincoln	20.27	30.56	14.00
Litke (Lütke)	−17.91	123.30	3.31
Lyman V	−63.46	151.44	2.46
Mädler	−10.90	31.80	6.10
Mandel'shtam-1 (S1)	5.89	161.47	4.20
Mandel'shtam-1 (S2)	5.78	161.48	1.79
Mandel'shtam-2	5.67	161.62	1.99
Mandel'shtam-3	6.83	161.03	11.77
Maurolycus-1	−41.79	14.84	1.50
Maurolycus-2	−41.58	14.40	4.00
McNally	20.65	231.22	7.11[c]
Milankovič-1 (S1)	77.06	158.26	5.90
Milankovič-1 (S2)	76.87	159.58	10.01
Milne-1 (S1)	−30.71	108.62	1.04
Milne-1 (S2)	−30.73	108.60	0.64
Milne-2	−31.04	108.09	1.42
Morozov (S1)	6.54	129.94	4.94
Morozov (S2)	6.77	130	3.03
Morse N	18.07	183.27	6.40
Nansen-1 (S1)	80.03	112.31	1.80
Nansen-1 (S2)	80.02	112.62	1.66
Nansen F	84.35	51.55	8.98
Oppenheimer F-1	−34.20	199.03	9.63
Oppenheimer F-2	−33.99	199.10	3.26
Paraskevopoulos H-1	48.68	213.01	5.39
Pasteur-1	−8.64	100.56	4.02
Pasteur-2	−8.22	100.74	1.90
Planck	−58.28	137.01	8.08
Poinsot	78.04	201.45	1.49
Poisson (S1)	−29.99	11.57	3.19
Poisson (S2)	−30.05	11.58	0.91
Racah B	−11.33	181.86	8.21
Racah X-1	−10.06	178.10	7.43[c]
Racah X-2	−9.50	178.22	11.24[c]
Racah X-3	−8.82	178.67	6.34[c]
Racah X-4	−8.55	178.76	5.98[c]
Racah X-5	−8.33	178.76	9.98[c]
Riphaeus	−6.86	331.49	13.28[c]
Rozhdestvenskiy-1	87.50	211.60	3.43
Rozhdestvenskiy-2 (S1)	87.01	181.58	7.06
Rozhdestvenskiy-2 (S2)	86.99	178.50	3.35
Sacrobosco	−24.50	16.92	2.88
Schaeberle-1 (S1)	−25.43	118.66	2.46
Schaeberle-1 (S2)	−25.30	118.70	1.69
Schaeberle-1 (S3)	−25.11	118.75	3.92
Seares	74.51	147.11	4.39
Shoemaker	−86.24	54.29	3.11
Simpelius-1	−73.56	13.04	1.00
Simpelius-2	−74.03	8.83	1.80
Simpelius-3	−73.92	9.90	3.24
Slipher	48.22	160.56	4.68
Van der Walls K-1	−46.64	120.70	4.63
Van der Walls K-2	−46.60	120.93	2.87
Virtanen	17.37	181.06	6.29
West Serenetatis	23.50	7.52	5.70[c]
Xenophanes (S1)	56.93	278.58	7.85
Xenophanes (S2)	56.59	278.56	8.87[c]

[a]Measurements were made using NAC mosaics unless otherwise indicated.

[b]Scarps are unofficially named after a large nearby crater or the crater within which they are located. The name is sometimes followed by a "-1," "-2," etc. to specify individual scarps within a cluster or complex of multiple individual scarps. "(S1)," "(S2)," etc. refers to separate segments of one individual scarp.

[c]The entire length of these lobate scarps is not yet covered by NAC images. This length measurement is an estimate based on NAC coverage combined with a WAC 100 m global mosaic

[d]Confirmed using the length measurement from *Binder and Gunga* [1985].

4 km) [i.e., *Watters et al.*, 1998; *Watters and Robinson*, 1999; *Watters et al.*, 2000; *Watters*, 2003; *Watters and Nimmo*, 2010; *Golombek and Phillips*, 2010]. Using the kinematic model described above, the same range in θ, and the maximum relief of the main scarp (60 m) [*Watters et al.*, 2011], the estimated horizontal shortening of Hinks Dorsum is ~70 to 170 m, a comparable result to that of the lunar lobate scarps.

[18] The frictional strength of the upper crust and megaregolith determines the stress necessary to initiate thrust faulting on the Moon. The minimum horizontal stress necessary to initiate faulting can be given by:

$$\Delta\sigma_{xx} = \frac{2f_s(\rho g z - p_w)}{\left(1 + f_s^2\right)^{1/2} - f_s}$$

where z is the depth of the fault, g is the acceleration due to gravity, ρ is the density of the crustal material, f_s is the coefficient of static friction, and p_w is the pore pressure which for the Moon, is set to zero [*Turcotte and Schubert*, 2002]. Because of the comparable scale and horizontal shortening expressed by lobate scarp segments on Eros, we

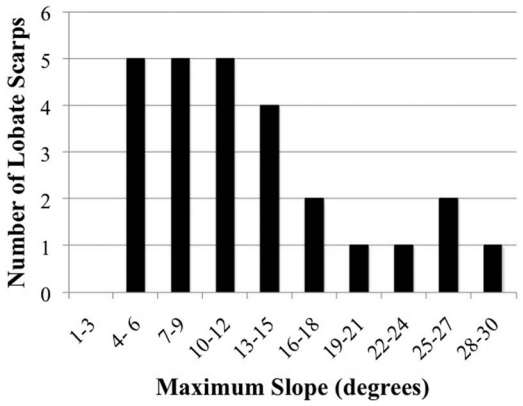

Figure 6. Histogram showing the distribution of the maximum slopes on scarp faces.

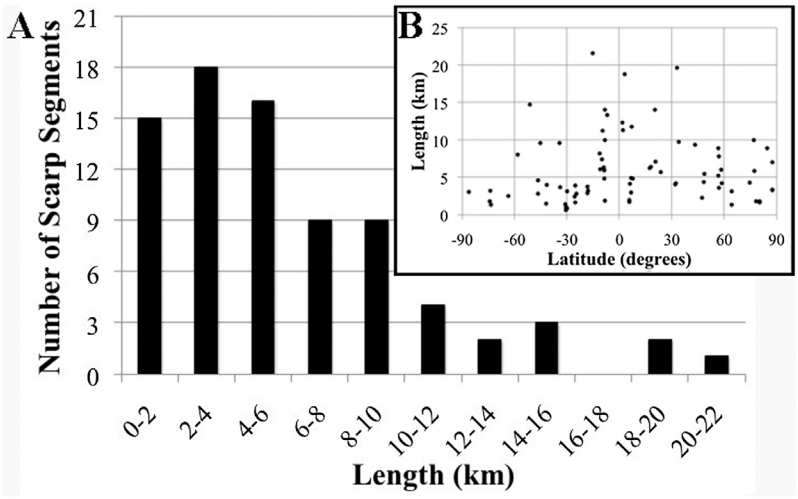

Figure 7. (a) Histogram showing the distribution of lobate scarp segment lengths. (b) Distribution of lobate scarp segment length by latitude.

use the modeled depth of these faults (maximum depth of ~240 m) [*Watters et al.*, 2011], to conservatively estimate a maximum depth of 1 km for the lunar lobate scarps. Laboratory measurements on the maximum shear stress needed to initiate movement as a function of normal stress are best fit by a maximum coefficient of friction of 0.85 for thrust faults, which corresponds to a fault plane dip of ~25° [*Byerlee*, 1977; *Turcotte and Schubert*, 2002]. Assuming failure in the upper lunar crust is controlled by the frictional strength [*Turcotte and Schubert*, 2002], we use lunar gravity of 1.63 m/s^2 [*Vaniman et al.*, 1991], an estimated megaregolith average density of 2700 kg/m^3, f_s = 0.85, and z = 1 km to estimate an upper limit for the near-surface shear strength of the Moon of roughly 16 MPa. Assuming there is no significant unexpressed contractional strain [*Watters et al.*, 2012], compressional stresses on the order of only ~16 MPa would be needed to initiate thrust faulting on the Moon. This level of stress is generally consistent with the estimated compressional stress reported by *Watters et al.* [2010] of less than 10 MPa.

4. Discussion

[19] Over time, the surface of the Moon has been subjected to local, regional, and global stresses. Basin-localized stresses have likely contributed to the formation of some of the lobate scarps, however their common occurrence in the lunar highlands and their apparent widespread distribution suggests that the source of the compressional stresses is predominantly global. Global sources of stress include reduction in spin rate [*Melosh*, 1980; *Helfenstein and Parmentier*, 1983; *Collins et al.*, 2010], tidal interactions with the Earth [*Gash*, 1978; *Melosh*, 1980; *Weber et al.*, 2009], and changes in volume due to thermal contraction

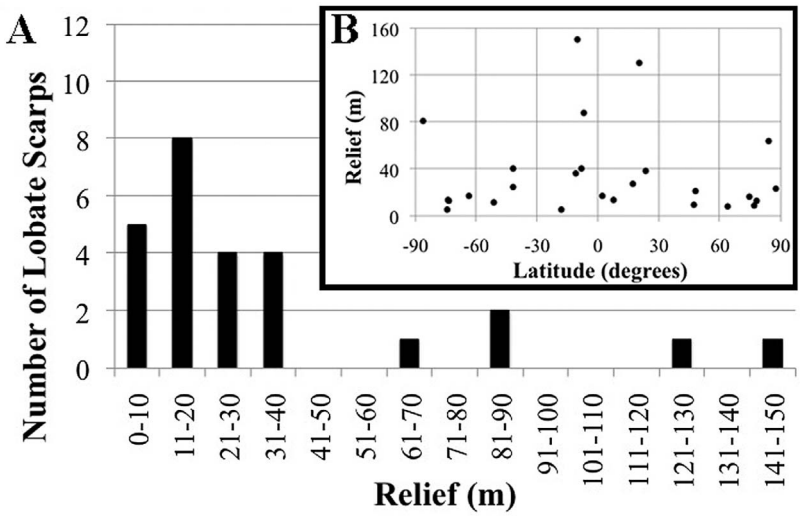

Figure 8. (a) Histogram showing the distribution of lobate scarp relief. (b) Distribution of lobate scarp relief by latitude.

of the interior [*Solomon and Chaiken*, 1976; *Binder and Lange*, 1977; *Solomon and Head*, 1979; *Binder*, 1982, 1986; *Solomon*, 1986]. Orbital recession of a tidally locked satellite, such as the Moon, may induce significant stresses [*Melosh*, 1980]. Despinning and tidal bulge reduction is predicted to cause a stress pattern with contraction and thrust faulting over a region extending ∼30° in latitude and longitude around the sub-Earth point and its antipode, extension and normal faulting near the poles, and horizontal shear stress in the midlatitudes [*Melosh*, 1980; *Helfenstein and Parmentier*, 1983; *Collins et al.*, 2010]. The currently observed spatial distribution of lobate scarps, particularly the occurrence of thrust faults in more than 20 different locations polewards of 60° latitude, is not consistent with this pattern [*Watters et al.*, 2010] (see Figure 2 and Tables 1 and 2). While tidal stresses raised solely by Earth are a likely component of the total stress forming the lobate scarps, the magnitude of the predicted stresses are only tens of kilopascals [*Weber et al.*, 2009]. Thus these tidal stresses by themselves are too weak to form the observed population of thrust faults [*Watters et al.*, 2010] which, as calculated above, are estimated to require compressional stresses on the order of ∼16 MPa for thrust faulting to be initiated. The relatively small amount of horizontal shortening and contractional strain expressed by the lobate scarps is consistent with thermal history models for an initially hot exterior, or magma ocean, that predict low-level compressional stresses (∼100 MPa or less) and a relatively small amount of late-stage radial contraction (∼1 km or less) due to secular cooling [*Solomon and Chaiken*, 1976; *Solomon and Head*, 1979; *Watters et al.*, 2010].

[20] The scale and horizontal shortening of individual lobate scarps are expressions of the amount of contractional strain. The order of magnitude difference in scale and range of S between lunar and Martian lobate scarps is consistent with larger amounts of strain associated with the Martian scarps [i.e., *Watters and Robinson*, 1999; *Watters et al.*, 2000; *Watters* 2003; *Grott et al.*, 2007]. On Mars, compressional stresses that formed the lobate scarps are thought to be a combination of stresses from the evolution of the crustal dichotomy boundary and global contraction [*Watters*, 1993; *Watters et al.*, 2007]. Lunar lobate scarps are comparable in scale and S to Hinks Dorsum [*Watters et al.*, 2011]. The origin of compressional stresses with sufficient magnitude to form thrust faults on Eros is still not well understood, but likely includes impact-induced compression [*Melosh*, 1989; *Richardson et al.*, 2004; *Thomas et al.*, 2001; *Watters et al.*, 2011]. Although we only have one example of a lobate scarp on an asteroid for comparison, the similar scale and range of S for lunar scarps and Hinks Dorsum suggest that perhaps differences in acceleration due to gravity may not be a major factor controlling the scale of the faults [see *Schultz et al.*, 2006].

[21] The population of lobate scarps on Mercury, like the Moon, is believed to have formed primarily from horizontally isotropic compressional stresses resulting from global radial contraction [i.e., *Strom et al.*, 1975; *Solomon and Chaiken*, 1976; *Cordell and Strom*, 1977; *Solomon and Head*, 1979; *Watters et al.*, 1998, 2010; *Solomon et al.*, 2008; *Watters and Nimmo*, 2010]. However, the greater scale and range of S estimated for the Mercurian scarps [*Watters et al.*, 1998, 2000, 2009; *Watters and Nimmo*, 2010], in comparison to estimates for the lunar scarps, is consistent with greater radial contraction. While estimates of global contractional strain for the Moon indicate a reduction in radius of ∼100 m [*Watters et al.*, 2010], estimates of the amount of contraction from the thrust faults on Mercury suggest a radius change of 1–2 km [*Strom et al.*, 1975; *Watters et al.*, 2009]. Thus while the source of the contractional strain on the Moon and Mercury both involve global contraction, the amount of predicted radius change differs by an order of magnitude or more. This likely reflects the very different thermal evolution of Mercury and the Moon [*Watters et al.*, 2010, 2012].

5. Summary and Conclusions

[22] LROC mosaics and stereo-derived digital terrain models (DTMs) and LOLA data are used to measure the relief and characterize the morphology of lobate scarps ranging in latitude from ∼86°S to 88°N and occurring on both the nearside and farside. The morphology of the relatively small-scale lunar lobate scarps, such as their characteristic asymmetric profiles and the range in maximum slope on scarp faces (∼5°–29°), is comparable to Hinks Dorsum on 433 Eros as well as the larger-scale planetary lobate scarps observed on Mars and Mercury [i.e., *Strom et al.*, 1975; *Watters*, 1993; *Watters and Robinson*, 1999; *Watters et al.*, 2000, 2009; *Watters and Johnson*, 2010; *Watters et al.*, 2011]. Relief of the lobate scarps ranges from ∼5 to 150 m with a mean relief of ∼35 m (median = ∼20 m, n = 26). Lengths of lobate scarp segments measured in LROC mosaics range from ∼0.6 to 21.6 km with a mean length of ∼6.0 km (median = 4.4 km; n = 79). Current data indicate that the lobate scarps as a whole typically exhibit tens of meters of relief and are tens of kilometers or less in length, consistent with previous estimates [*Binder and Gunga*, 1985; *Watters and Johnson*, 2010]. Estimated lower limits for the horizontal shortening expressed by the lobate scarp thrust faults range from ∼10 to 410 m for a range in θ of 20° to 40°. The scale and horizontal shortening of lunar scarps is generally an order of magnitude lower than estimates for planetary lobate scarps, but comparable to estimates for Hinks Dorsum [i.e., *Strom et al.*, 1975; *Watters et al.*, 1998, 2000, 2009, 2011; *Watters*, 2003; *Watters and Nimmo*, 2010]. The relatively low maximum relief and small amount of horizontal shortening estimated for the measured scarps is consistent with a small amount of global radial contraction. A low level of isotropic compressional stress due to a small amount of radial contraction is consistent with the low levels of compressional stress needed to initiate shallow-rooted thrust faults on the Moon.

[23] **Acknowledgments.** We gratefully acknowledge the LRO and LROC engineers and technical support personnel. This work benefited from thoughtful reviews by Ernst Hauber, Matthew Golombek, and Laurent Montesi. This work was supported by NASA Grant NNX08AM73G.

References

Banks, M. E., T. R. Watters, M. S. Robinson, J. F. Bell III, M. E. Pritchard, N. R. Williams, K. Daud, and the LROC team (2011), The search for lunar lobate scarps using images from the Lunar Reconnaissance Orbiter Camera, *Lunar Planet. Sci.*, *XLII*, Abstract 2736.

Binder, A. B. (1982), Post-Imbrian global lunar tectonism: Evidence for an initially totally molten Moon, *Earth Moon Planets*, *26*, 117–133, doi:10.1007/BF00929277.

Binder, A. B. (1986), The initial thermal state of the Moon, in *Origin of the Moon*, edited by W. K. Hartmann, R. J. Phillips, and G. J. Taylor, pp. 425–433, Lunar and Planet. Inst., Houston, Tex.

Binder, A. B., and H.-C. Gunga (1985), Young thrust-fault scarps in the highlands: Evidence for an initially totally molten Moon, *Icarus*, *63*, 421–441, doi:10.1016/0019-1035(85)90055-7.

Binder, A. B., and M. Lange (1977), On the thermal history of a Moon of fission origin, *Moon*, *17*, 29–45, doi:10.1007/BF00566851.

Brewer, J. A., S. B. Smithson, J. E. Oliver, S. Kaufman, and L. D. Brown (1980), The Laramide orogeny: Evidence from COCORP deep crustal seismic profiles in the Wind River mountains, Wyoming, *Tectonophysics*, *62*, 165–189, doi:10.1016/0040-1951(80)90191-2.

Byerlee, J. (1977), Friction of rocks, in *Experimental Studies of Rock Friction with Application to Earthquake Prediction*, edited by J. F. Evernden, pp. 55–77, U.S. Geol. Survey, Menlo Park, Calif.

Byerlee, J. (1978), Friction of rocks, *Pure Appl. Geophys.*, *116*, 615–626, doi:10.1007/BF00876528.

Collins, G. C., W. B. McKinnon, J. M. Moore, F. Nimmo, R. T. Pappalardo, L. M. Prockter, and P. M. Schenk (2010), Tectonics of the outer satellites, in *Planetary Tectonics*, edited by T. R. Watters and R. S. Schultz, pp. 264–350, Cambridge Univ. Press, New York.

Cordell, B. M., and R. G. Strom (1977), Global tectonics of Mercury and the Moon, *Phys. Earth Planet. Inter.*, *15*, 146–155, doi:10.1016/0031-9201(77)90027-9.

Gash, P. J. S. (1978), Tidal stresses in the Moon's crust, *Mod. Geol.*, *6*, 211–220.

Golombek, M. P., and R. J. Phillips (2010), Mars tectonics, in *Planetary Tectonics*, edited by T. R. Watters and R. S. Schultz, pp. 183–232, Cambridge Univ. Press, New York.

Golombek, M. P., J. B. Plescia, and J. B. Franklin (1991), Faulting and folding in the formation of planetary wrinkle ridges, *Proc. Lunar Planet. Sci. Conf.*, *21st*, 679–693.

Golombek, M. P., F. S. Anderson, and M. T. Zuber (2001), Martian wrinkle ridge topography: Evidence for subsurface faults from MOLA, *J. Geophys. Res.*, *106*, 23,811–23,821.

Gries, R. (1983), Oil and gas prospecting beneath Precambrian of foreland thrust plates in Rocky Mountains, *Am. Assoc. Pet. Geol. Bull.*, *67*, 1–28.

Grott, M., E. Hauber, S. C. Werner, P. Kromberg, and G. Neukum (2007), Mechanical modeling of thrust faults in the Thaumasia region, Mars, and implications for the Noachian heat flux, *Icarus*, *186*, 517–526, doi:10.1016/j.icarus.2006.10.001.

Helfenstein, P., and E. M. Parmentier (1983), Patterns of fracture and tidal stresses on Europa, *Icarus*, *53*, 415–430, doi:10.1016/0019-1035(83)90206-3.

Howard, K. A. and W. R. Muehlberger (1973), Lunar thrust faults in the Taurus-Littrow region, *NASA Spec. Publ.*, *SP-330*, 31-22–31-25.

Jaeger, J. C., and N. G. W. Cook (1979), *Fundamentals of Rock Mechanics*, 3rd ed., 593 pp., Chapman and Hall, New York, doi:10.1017/CBO9780511735349.

Lucchitta, B. K. (1976), Mare ridges and related highland scarps: Results of vertical tectonism, *Geochim. Cosmochim. Acta*, *3*, suppl., 2761–2782.

Lucchitta, B. K. (1977), Topography, structure, and mare ridges in southern Mare Imbrium and northern Oceanus Procellarum, *Proc. Lunar Sci. Conf.*, *8th*, 2691–2703.

Masursky, H., G. W. Colton, and F. El-Baz (1978), *Apollo Over the Moon: A View From Orbit*, *NASA Spec. Publ.*, *SP-362*, 255 pp.

Mattingly, T. K., F. El-Baz, and R. A. Laidley (1972), Observations and impressions from lunar orbit, *NASA Spec. Publ.*, *SP-315*, 28-1–28-16.

Melosh, H. J. (1980), Tectonic patterns on a tidally distorted planet, *Icarus*, *43*(3), 334–337, doi:10.1016/0019-1035(80)90178-5.

Melosh, H. J. (1989), *Impact Cratering*, 245 pp., Oxford Univ. Press, New York.

Plescia, J. B., and M. P. Golombek (1986), Origin of planetary wrinkle ridges based on the study of terrestrial analogs, *Geol. Soc. Am. Bull.*, *97*, 1289–1299.

Richardson, J. E., H. J. Melosh, and R. Greenberg (2004), Impact-induced seismic activity on asteroid 433 Eros: A surface modification process, *Science*, *306*, 1526–1529, doi:10.1126/science.1104731.

Robinson, M. S., et al. (2010), Lunar Reconnaissance Orbiter Camera instrument overview, *Space Sci. Rev.*, *150*, 81–124, doi:10.1007/s11214-010-9634-2.

Scholten, F., J. Oberst, K.-D. Matz, T. Roatsch, M. Wählisch, E. J. Speyerer, and M. S. Robinson (2012), GLD100: The near-global lunar 100 meter raster DTM from LROC WAC stereo image data, *J. Geophys. Res.*, doi:10.1029/2011JE003926, in press.

Schultz, P. H. (1976), *Moon Morphology: Interpretations based on Lunar Orbiter Photography*, 626 pp., Univ. of Texas Press, Austin, Tex.

Schultz, R. A. (2000), Localization of bedding-plane slip and back-thrust faults above blind thrust faults: Keys to wrinkle ridge structure, *J. Geophys. Res.*, *105*, 12,035–12,052.

Schultz, R. A., and T. R. Watters (2001), Forward mechanical modeling of the Amenthes Rupes thrust fault on Mars, *Geophys. Res. Lett.*, *28*, 4659–4662, doi:10.1029/2001GL013468.

Schultz, R. A., C. H. Okubo, and S. J. Wilkins (2006), Displacement-length scaling relations for faults on the terrestrial planets, *J. Struct. Geol.*, *28*, 2182–2193, doi:10.1016/j.jsg.2006.03.034.

Smith, D. E., et al. (2010), The Lunar Orbiter Laser Altimeter investigation on the Lunar Reconnaissance Orbiter mission, *Space Sci. Rev.*, *150*, 209–241, doi:10.1007/s11214-009-9512-y.

Solomon, S. C. (1986), *Origin of the Moon*, edited by W. K. Hartmann, R. J. Phillips, and G. J. Taylor, pp. 311–329, Lunar and Planet. Inst., Houston, Tex.

Solomon, S. C., and J. Chaiken (1976), Thermal expansion and thermal stress in the Moon and terrestrial planets: Clues to early thermal history, *Proc. Lunar Sci. Conf.*, *7th*, 3229–3243.

Solomon, S. C., and J. W. Head (1979), Vertical movement in mare basins: Relation to mare emplacement, basin tectonics, and lunar thermal history, *J. Geophys. Res.*, *84*, 1667–1682, doi:10.1029/JB084iB04p01667.

Solomon, S. C., et al. (2008), Return to Mercury: A global perspective on MESSENGER's first Mercury flyby, *Science*, *321*, 59–62, doi:10.1126/science.1159706.

Stone, D. S. (1985), Geologic interpretation of seismic profiles, Big Horn Basin, Wyoming, Part I: East flank, in *Seismic Exploration of the Rocky Mountain Region*, edited by R. R. Gries and R. C. Dyer, pp. 165–174, Rocky Mt. Assoc. of Geol., Denver, Colo.

Strom, R. G. (1972), Lunar mare ridges, rings, and volcanic ring complexes, *Mod. Geol.*, *2*, 133–157.

Strom, R. G., N. J. Trask, and J. E. Guest (1975), Tectonism and volcanism on Mercury, *J. Geophys. Res.*, *80*, 2478–2507, doi:10.1029/JB080i017p02478.

Thomas, P. C., et al. (2001), Shoemaker crater as the source of most ejecta blocks on the asteroid 433 Eros, *Nature*, *413*, 394–396, doi:10.1038/35096513.

Tran, T., et al. (2010), Generating digital terrain models using LROC NAC images, paper presented at a special joint symposium of ISPRS Technical Commission IV and AutoCarto in conjunction with ASPRS/CaGIS 2010 Fall Specialty Conference, Orlando, Fla., 15–19 November.

Turcotte, D. L., and G. Schubert (2002), *Geodynamics*, 2nd ed., edited by D. L. Turcotte and G. Schubert, 456 pp., Cambridge Univ. Press, New York.

Vaniman, D., R. Reedy, G. Heiken, G. Olhoeft, and W. Mendell (1991), The lunar environment, in *Lunar Sourcebook*, edited by G. H. Heiken, D. T. Vaniman, and B. M. French, pp. 27–60, Cambridge Univ. Press, Cambridge, New York.

Watters, T. R. (1988), Wrinkle ridge assemblages on the terrestrial planets, *J. Geophys. Res.*, *93*, 10,236–10,254.

Watters, T. R. (1993), Compressional tectonism on Mars, *J. Geophys. Res.*, *98*, 17,049–17,060, doi:10.1029/93JE01138.

Watters, T. R. (2003), Thrust faults along the dichotomy boundary in the eastern hemisphere of Mars, *J. Geophys. Res.*, *108*(E6), 5054, doi:10.1029/2002JE001934.

Watters, T. R. (2004) Elastic dislocation modeling of wrinkle ridges on Mars, *Icarus*, *171*, 284–294.

Watters, T. R., and C. L. Johnson (2010), Lunar tectonics, in *Planetary Tectonics*, edited by T. R. Watters and R. S. Schultz, pp. 121–182, Cambridge Univ. Press, New York.

Watters, T. R., and F. Nimmo (2010), The tectonics of Mercury, in *Planetary Tectonics*, edited by T. R. Watters and R. A. Schultz, pp. 15–80, Cambridge Univ. Press, New York.

Watters, T. R., and M. S. Robinson (1999), Lobate scarps and the Martian crustal dichotomy, *J. Geophys. Res.*, *104*, 18,981–18,990, doi:10.1029/1998JE001007.

Watters, T. R., and R. A. Schultz (2002), The fault geometry of planetary lobate scarps: Listric versus planar, *Proc. Lunar Planet. Sci. Conf.*, *33rd*, 1668.

Watters, T. R., M. S. Robinson, and A. C. Cook (1998), Topography of lobate scarps on Mercury: New constraints on the planet's contraction, *Geology*, *26*, 991–994, doi:10.1130/0091-7613(1998)026<0991:TOLSOM>2.3.CO;2.

Watters, T. R., R. A. Schultz, and M. S. Robinson (2000), Displacement-length relations of thrust faults associated with lobate scarps on Mercury and Mars: Comparison with terrestrial faults, *Geophys. Res. Lett.*, *27*, 3659–3662, doi:10.1029/2000GL011554.

Watters, T. R., R. A. Schultz, M. S. Robinson, and A. C. Cook (2002), The mechanical and thermal structure of Mercury's early lithosphere, *Geophys. Res. Lett.*, *29*(11), 1542, doi:10.1029/2001GL014308.

Watters, T. R., P. J. McGovern, and R. P. Irwin III (2007), Hemispheres apart: The crustal dichotomy on Mars, *Annu. Rev. Earth Planet. Sci.*, *35*(1), 621–652, doi:10.1146/annurev.earth.35.031306.140220.

Watters, T. R., S. C. Solomon, M. S. Robinson, J. W. Head, S. L. André, S. A. Hauck II, and S. L. Murchie (2009), The tectonics of Mercury: The view after MESSENGER's first flyby, *Earth Planet. Sci. Lett.*, *285*, 283–296, doi:10.1016/j.epsl.2009.01.025.

Watters, T. R., et al. (2010), Evidence of recent thrust faulting on the Moon revealed by the Lunar Reconnaissance Orbiter Camera, *Science*, *329*, 936–940, doi:10.1126/Science.1189590.

Watters, T. R., P. C. Thomas, and M. S. Robinson (2011), Thrust faults and the near-surface strength of asteroid 433 Eros, *Geophys. Res. Lett.*, *38*, L02202, doi:10.1029/2010GL045302.

Watters, T. R., M. S. Robinson, M. E. Banks, T. Tran, and B. W. Denevi (2012), Recent extensional tectonics on the Moon revealed by the Lunar Reconnaissance Orbiter camera, *Nat. Geosci.*, *5*, 181–185, doi:10.1038/NGEO1387.

Weber, R. C., B. G. Bills, and C. L. Johnson (2009), Constraints on deep moonquake focal mechanisms through analyses of tidal stresses, *J. Geophys. Res.*, *114*, E05001, doi:10.1029/2008JE003286.

Wilhelms, D. E. (1987), *The Geologic History of the Moon*, U. S. Govt. Print. Off., Washington, D. C.

Wojtal, S. F. (1996), Changes in fault displacement populations correlated to linkage between faults, *J. Struct. Geol.*, *18*, 265–279, doi:10.1016/S0191-8141(96)80049-6.

Wolfe, E. W., N. G. Bailey, B. K. Lucchitta, W. R. Muehlberger, D. H. Scott, R. L. Sutton, and H. G. Wilshire (1981), The geologic investigation of the Taurus-Littrow Valley: Apollo 17 landing site, *U.S. Geol. Surv. Prof. Pap.*, *1080*, 280 pp.

M. E. Banks, L. L. Tornabene, and T. R. Watters, Center for Earth and Planetary Studies, National Air and Space Museum, Smithsonian Institution, Washington, DC 20560, USA. (banksme@si.edu)

L. Ojha, Lunar and Planetary Laboratory, University of Arizona, Tucson, AZ 85721, USA.

M. S. Robinson, T. Tran, and N. R. Williams, School of Earth and Space Exploration, Arizona State University, Tempe, AZ 85287, USA.